Fine structure of cell wall surfaces in the giant-cellular xanthophycean alga *Vaucheria terrestris*

Ichiro Mine and Kazuo Okuda.

Graduate School of Kuroshio Science, Kochi University

2-5-1, Akebono-cho, Kochi 780-8520 Japan

Corresponding author: Ichiro Mine

email address: mine@cc.kochi-u.ac.jp

Telephone number: +81-88-844-8309

Fax number: +81-88-844-8356

Abstract

The mechanical strength of cell walls in the tip-growing cells of *Vaucheria terrestris* is weakened by treatment with proteolytic enzymes. To clarify the morphological characteristics of the components maintaining cell wall strength, the fine structures of the cell walls, with and without protease treatment, were observed by transmission electron microscopy and atomic force microscopy. Observations indicated that cellulose microfibrils were arranged in random directions and overlapped each other. Most of the microfibrils observed in the inner surface of the cell wall were embedded in amorphous materials, whereas in the outer surface of the cell wall microfibrils were partially covered by amorphous materials. The matrix components embedding and covering microfibrils were almost completely removed by protease treatment, revealing layers of naked microfibrils deposited deeply in the cell wall. Topographic data taken from atomic force microscopic observations provided some additional information that could not be obtained by transmission electron microscopy, including more detailed images of the granular surface textures of the matrix components and the detection of microfibrils in the interior of the cell wall. In addition, quantitative atomic force microscopy data of local surface heights enabled us to draw three-dimensional renderings and to quantitatively estimate the extent of the exposure of microfibrils by the enzymatic treatment.

Keywords: Cell wall, Cellulose microfibril, Electron microscopy, Metal shadowing, Replica, Atomic force microscopy

Introduction

The cell wall of plants, algae, and fungi is a thin but rigid extracellular structure that covers the entire surface of cells. Usually, high tensile stress due to the cell turgor pressure is applied to the cell wall and the extension of an existing cell wall under such tensile stress is believed to be involved in cell growth (Cosgrove 1997). Therefore, the mechanical properties such as extensibility and strength of the cell wall are considered to be important factors for cell growth and morphogenesis. A number of studies have shown a correlation between growth rates and cell wall extensibility in the multicellular tissues of angiosperms that exhibit diffuse growth, in which cell growth is not localized to a specific part of the cell (Masuda 1990; Kutschera 1991; Cosgrove 1993). In such plant cells, it has been postulated that the mechanical properties of cell walls are controlled by the modification of matrix components by cell wall proteins (Cosgrove 1999). These proteins include expansin, which acts on hydrogen bonds between cellulose microfibrils and the load-bearing hemicellulose (Cosgrove 1996), xyloglucan endotransglycosylase, which cuts and grafts the backbone glucan chains of xyloglucans (Nishitani 1997; Rose et al. 2002), and specific cellulases that potentially affect the association of hemicellulose with cellulose microfibrils (Park et al. 2003).

We have reported previously that the growing tip is the most extensible region in the tip-growing cells of the giant cellular alga *Vaucheria terrestris*, in which cell expansion is limited to a domed end of the cylindrical cell (Mine and Okuda 2003). Moreover, the cell wall is significantly weakened by treatment with some proteases, such as subtilisin, and the protease-treated cell wall shows a transverse expansion in the cylindrical region rather than expansion in the growing tip. This implies that some proteinaceous components are responsible for the mechanical strength of the cell wall,

which is important for maintaining the cylindrical cell shape even under the high cell wall stress in the hoop direction. In order to identify and determine the structure of the cell wall components in this alga, it is necessary to observe the fine structures of both intact and protease-treated cell walls, particularly the structures of matrix components and cellulose microfibrils.

The fine structures of cellulose microfibrils and matrix components have been observed on shadowed replicas of rapid-frozen and deep-etched wall specimens by transmission electron microscopy (McCann et al. 1990, 1991; Fujino et al. 2000). The high resolution of transmission electron microscopy and metal-shadowing techniques have provided insights into the three-dimensional structure of microfibrils and other cell wall components and is generally regarded as more convincing than other methods such as thin sectioning for transmission electron microscopy .

Since its invention in 1986 (Binnig et al. 1986), atomic force microscopy has been developed for obtaining topographic images of specimen surfaces at atomic resolution. Topographic images are obtained by tracing the height of specimen surfaces with the fine tip of a probe that scans the specimen area. Therefore, atomic force microscopy can provide a three-dimensional surface structure with the actual height of each scanned point, whereas a shadowing method for transmission electron microscopy provides the image contrasts only according to the slope of the specimen surfaces. Furthermore, atomic force microscopic observations can be carried out readily on specimens under atmospheric conditions, whereas transmission electron microscopy specimens or replicas must be kept under high vacuum. Thus, atomic force microscopy has the potential to provide “real” topographic data of the surface of biological specimens without artifacts due to specimen preparation or high vacuum environments. A number of

investigations using atomic force microscopy have been carried out on biological specimens (Hörber and Miles 2003 for review; Morris et al. 2004). Cell walls are adequate biological materials for atomic force microscopic observations because they are relatively rigid and might not be destroyed by contact with the probe tip during scanning. Therefore, there have been a number of reports of atomic force microscopy of plant cell wall structures (Kirby et al. 1996; Round et al. 1996; Pesacreta et al. 1997; Thimm et al. 2000) and comparisons of cell wall structures before and after extraction of matrix polysacchride has been also carried out (Davies and Harris 2003).

In the present study, we examine the fine structure of cell wall surfaces in the giant cell of *V. terrestris*, with or without protease treatment, in order to explore the structures involved in the maintenance of cell wall strength. Three-dimensional fine structures of cell wall components were observed by atomic force microscopy of air-dried specimens in an ambient atmosphere at a resolution of a few nanometers, as well as by transmission electron microscopy of shadowed replicas. Quantitative topographic data obtained from atomic force microscopic observations were used to generate three-dimensional renderings of the cell wall structure, allowing the recognition of the fine structural features and the extraction and quantification of ridge-like structures in order to estimate the exposure of cellulose microfibrils quantitatively.

Materials and methods

Algal material

A unialgal strain of *V. terrestris* sensu Götz was obtained from Dr. Hironao

Kataoka (Tohoku University, Sendai, Japan) and cultured as described previously (Mine and Okuda 2003).

Buffer and enzyme solution

The experimental buffer was a mixture of 20 mM Tris(hydroxymethyl)aminomethane and 20 mM 2-morpholinoethanesulfonic acid (pH 7.0). The proteolytic enzyme (P8038; subtilisin Carlsberg; Lot No. 21K1653, purchased from Sigma) was suspended in the buffer at a concentration of 10 Units ml^{-1} for protease treatment of cell wall fragments.

Preparation of cell wall fragments

The growing tip regions of *V. terrestris* cells were isolated and the protoplasm was removed to obtain apical cell wall fragments (0.2-0.5 mm in length), as described previously (Mine and Okuda 2003). These apical cell wall fragments were washed with the buffer three times. To observe the inner surface of the cell wall, in some fragments, the apical portion was turned inside-out (figs 1a-c) using a pair of glass needles made from glass tubes (GD-1, Narishige Scientific Instrument Laboratory, Tokyo) with a needle puller (PC-10, Narishige) and a microforge (MF-900, Narishige).

Protease treatment

Protease treatment was carried out by incubating cell wall fragments, both right-side-out and inside-out, in the buffer solution containing protease, prepared as described above, at $30^{o}C$ for 24 h. After the protease treatment, the cell wall fragments were washed three times with distilled water. Control experiments were carried out using

the autoclave-inactivated enzyme, with the same results as with no enzymatic treatment (data not shown).

Regions of observation

The four types of cell wall fragments, i.e., right-side-out/no treatment, right-side-out/protease-treated, inside-out/no treatment, and inside-out/protease-treated, were air-dried on glass cover slips for atomic force microscopic observation and on acetyl cellulose sheets for replica preparations. The cylindrical portion of the cell wall fragment was almost entirely flat, with only a few undulations, whereas the hemispherical portion was notably undulated (Fig. 1d). As diagrammed in Fig. 1e, the apical cell wall surface was divided into the following three regions: (A) apical region including the apex and dome; (B) intermediate region just behind the apical region; and (C) cylindrical region. Since there are significant spatial differences in growth rate (Kataoka 1982) and cell wall extensibility (Mine and Okuda 2003) between the young cell surface in the tip region and the older surface in the cylindrical region, comparative observations of the celll wall structures were made from these regions.

Preparation and observation of atomic force microscopy specimens

Cell wall fragments were immobilized on a glass cover slip pretreated with aqueous polyethyleneimine P-70 solution (Wako Pure Chemicals, Osaka; original 30% solution diluted 1:300 with distilled water), air-dried, and observed by atomic force microscopy with a JEOL JSPM-4200 at the Industrial Technology Center of Kochi Prefecture, Japan, using the AC mode with a probe (OMCL-AC160TS-C2, Olympus Co., Tokyo). The nominal spring constant and resonance were 42 N m^{-1} and 300 kHz,

respectively. Topographic images (512 x 512 pixels, TIFF format) of the cell wall fragments were obtained by scanning a 1 x 1 μm specimen area. Scanning speed was 0.67 ms per pixel. Other scanning conditions were unchanged from the preset conditions.

Image processing

The three-dimensional renderings were obtained with the Scanning Probe Image Processor for Windows, Version 3.2.3.0 (SPIP demonstration version, Image Metrology A/S, Lyngby, Denmark) from a 128 x 128 pixel (250 x 250 nm) portion excised from the topographic images using computer software (Scion Image, Scion Corporation, Frederick, MD, USA).

After the cell wall matrix components were removed, a number of fibrous structures were exposed. In order to quantify the fibrous structures that were exposed, ridge extraction was carried out using a custom-made macro procedure for Scion Image. This calculated the height of each pixel in the lowered resolution (128 x 128 pixels) topographic images and selected the "peak pixels," which were more than 0.5 nm higher than the average heights of the right and left and above and below pixels. The macro procedure further examined all of the peak pixels and extracted the "neighbored peaks," which had one or more peak pixel among the four neighboring (right, left, above, and below) pixels. The number of the neighbored peaks divided by the total pixel number and the sum of the numbers of the neighboring peak pixels out of all of the neighbored peaks in the entire image were designated as the "neighbored peak ratio" and the "peak neighboring index," respectively. These two indices, calculated from the 78 topographic data, showed a very strong correlation (r^2 of a liner regression was 0.98). Therefore, only the neighbored peak ratios are shown in the Results.

Unstable scanning with atomic force microscopy often resulted in horizontal discontinuities in topographic images and therefore continuous horizontal lines of the peak pixels, regardless of the specimen surface morphology. In such cases, the discontinuities were removed by an offset-flattening filter of the image-processing software (WSxM, Nanotech Electronica, Madrid, Spain) before peak analyses. After applying this filter, the changes in the above indices that were unrelated to the discontinuities were further calibrated by the average changes occurring in 10 other images without such discontinuities.

Preparation and observation of shadowed replica

Cell wall fragments were transferred onto an acetyl cellulose sheet and allowed to dry for several s after removing excess water with filter paper. Immediately after drying, a small piece of the sheet with the dried cell wall fragment was excised and adhered to a copper specimen holder with a small amount of starch glue. The specimen was frozen on the precooled specimen stage of a freeze-etching device (FD-3, Eiko Engineering Co., Mito, Japan) and shadowed with platinum-carbon and reinforced by evaporating carbon. . Rotary shadowing at an angle of 30º was conducted for 25-40 s at 4-6 x 10^{-7} Pa. The specimen temperature was about -110ºC as read from the built-in thermometer.

After evaporation, the specimen was warmed to room temperature, transferred to ambient atmosphere, removed from the specimen holder, and floated on 70% sulfuric acid at 70ºC for two days to decompose the acetyl cellulose sheet and the cell wall. The sulfuric acid was changed once during the decomposition. The replica was then floated on 2.5% sodium dichromate at room temperature for 10 min, washed with distilled water

three times, and collected on a single-slot copper grid supported by a formvar membrane. Specimens were observed with a JEOL JEM-1010T and photographed on negative film (FG 5.9 x 8.2 cm, Fuji Photographic Film Co., Tokyo). After image development, the electron micrographs were converted to grayscale digital images with a film scanner (Dimage Scan Multi, Minolta, Tokyo) and the colors were inverted using Adobe Photoshop 5.0 Limited Edition.

Preparation, observation, and measurement of isolated cellulose microfibrils

Cells were harvested and homogenized in a blender and cell walls were separated from the cytoplasm by three centrifugations followed by suspension in distilled water. After sonication by a ultrasonic processor (VP-5, Taitec Corp., Tokyo , Japan) for 1 min, precipitated cell wall fragments were incubated for 5 min in an acetic-nitric reagent (Updegraff 1969) in a boiling-water bath to remove non-cellulosic components of the cell wall. The remaining solids were washed by re-suspension in distilled water followed by centrifugation three times and stored at –80ºC until observation. For transmission electron microscopic observations, the CMFs were thawed and air-dried on a formvar-supported, 100-mesh copper grid, negatively-stained with 1% aqueous uranyl acetate, and observed and photographed by transmission electron microscopy at 10,000X magnification, as described above. The thickness and width of the isolated CMFs were directly measured with a ruler under a dissecting microscope on 4X-enlarged prints of the negative films. For atomic force microscopic observations, isolated CMFs were air-dried on a cover slip and topographic images were obtained as described above. The thickness and width of the isolated CMFs were measured on the topographic images using Scion Image. An outline of a CMF cross-section was obtained as a “line profile” along a line

crossing the CMF at a right angle and a straight bottom line connecting the right and left ends of the convex outline of the CMF that was drawn manually. The point farthest from the bottom line on the CMF outline was determined and the distance between the point and the bottom line was taken as the thickness of the CMF. The distance between the two intersections of the CMF outline with the halfway line between the point and the bottom line was measured as the width of the CMF (cf Fig. 9c).

Results

The observations were carried out on the natural outer cell-wall surfaces as well as the inner surfaces prepared from inside-out wall fragments. The procedure of turning the cell walls inside out is shown in detail in Fig. 1a-1c. In addition, the observations were performed in the apical, intermediate, and more basal cylindrical regions of the alga (Fig. 1e).

Inner surface of intact cell walls

Inner surfaces of inside-out apical cell wall fragments were observed by atomic force microscopy (Figs. 2a-c) and by transmission electron microscopy (Figs. 2d-f). In the topographic images, broadly extended dark and bright fields indicated rough vertical undulations on the cell wall surface (Figs. 2a-c). These undulations were not recognizable in the shadowed replicas of similar cell wall specimens (Figs. 2d-f). Cellulose microfibrils were arranged in various directions in the superficial layer (Fig. 2). No specific tendencies or patterns were recognizable. Microfibrils were dense and

overlapping in the cylindrical region (Figs. 2c, 2f), but sparse in the apical region where areas between microfibrils were covered by amorphous materials (Figs. 2a, 2d). Given that cell wall components are generally divided into two categories, skeletal and matrix, the amorphous materials may fall into the latter category. Hereafter, we refer to such amorphous materials as the matrix components of the cell walls of this alga. In both atomic force microscopy and transmission electron microscopy specimens, microfibrils in the intermediate region of the cell wall showed densities that were intermediate between those of the apical and cylindrical regions (Figs. 2b, 2e).

The superficial microfibrils on the inner surface of the cylindrical cell wall, which is older than the apical cell wall, were denser than those of the apical cell wall. This indicates that microfibrils are continuously deposited over existing microfibrils as the apical wall is displaced from the cell apex to the cylindrical region. In addition, the matrix components present under the superficial microfibrils appeared to have fine granules in the atomic force microscopy specimens as indicated by arrows in Fig. 2a, whereas they appear rather smooth in the shadowed replicas (Fig. 2d). Thus, the surface texture of these components could be viewed in more detail by atomic force microscopy than in shadowed replicas.

Outer surface of intact cell walls

As shown in Fig. 3, the outer surfaces of the cell wall fragments showed very different configurations than the inner surfaces. A number of cellulose microfibrils overlapped and the direction and arrangement of microfibrils were random. Irregular-shaped matrix components partially covered the surfaces of the wall and embedded the outermost microfibril layer but microfiblis in deeper layer were not

embedded in the matrix components as in the inner surface of the cell wall (Fig. 3).

Atomic foce microscopic observations revealed that the matrix components covering the outermost microfibril layers exhibited irregularly granular undulations (Figs. 3a, b). In contrast, in the specimens for transmission electron microscopy the surface of the matrix components of the outer cell wall surface appeared to be smooth rather than granular (Figs. 3d-f). The granular undulations observed in the topographic images probably reflect the compression of the densely crossing microfibrils under the matrix components against each other beneath the probe as the sample was scanned. Judging from the number of fibrous structures that could be detected, the coverage of microfibril layers by these matrix components was greater in the cylindrical region (Figs. 3c, f) than in the other two regions (Figs. 3a, b, d, e), implying that the materials developed as the cell wall stopped expanding.

Protease-treated cell walls

Protease treatment caused the partial removal of matrix components in both the inner and the outer surfaces of cell walls. In the inner surface, the amorphous matrix components under the superficial cellulose microfibrils were removed by the treatment (Fig. 4), revealing many overlapping microfibrils present deeply in the wall. Before the treatment these microfibrils had probably been embedded in the matrix components. In specimens for atomic force microscopy (Figs. 4a-c), the microfibrils in very deep layers of the cell wall could be detected and the surfaces of individual microfibrils appeared to be smooth. Concomitantly, vertical rough undulation was not obvious on the surface of the protease-treated cell walls probably due to the loss of the matrix components concerning with the integrity of the cell wall. In the cylindrical region, the matrix

components were almost completely removed (Fig. 4c), but some fine granular matrix components remained in the cell walls of the apical and intermediate regions (Figs. 4a, b). In the shadowed replicas (Figs. 4d-f), however, such granular structures were not detectable and it was difficult to distinguish the gaps between microfibrils from the remnants of amorphous matrix components without local height information of the specimen surface. The protease treatment also resulted in small dark holes in the shadowed replicas, which were probably due to exposure of small parts of the cell wall which were too deep to be evaporated by the metal during shadowing. The number and total area of these dark holes were larger in the cylindrical region (Fig. 4f) than in the apical (Fig. 4d) and intermediate (Fig. 4e) regions, indicating that the matrix components were removed more extensively in the cylindrical region than in other regions.

On the outer surface of the protease-treated cell walls, the irregular-shaped matrix components were almost completely removed, resulting in the visualization of many layers of randomly arranged microfibrils, both in the atomic force microscopy specimens (Fig. 5) and in the shadowed replicas (not shown).

Three-dimensional and ridge extraction of atomic force microscopy images

Figure 6 shows the three-dimensional renderings, which were selected from the topographic images shown in Figs. 2-5. Some of the features in the topographic images were enhanced and more recognizable in these pictures. The coarse, vertical undulation of the surfaces is more conspicuous in intact cell walls (Figs. 6a-d) than in protease-treated cell walls (Figs. 6e-h). The coverage of microfibril layers with rough granular undulations are distinct in Figs. 6c and 6d.

Comparison of the atomic force microscopy or transmission electron

microscopy images of intact cell walls and of those treated with the protease showed that the protease treatment resulted in the removal of matrix components that had embedded or covered microfibrils. We tried to quantitatively estimate the emergence of fibrous structures such as microfibrils by extracting ridge-like structures as continuous local peak pixels from the low-resolution topographic images. Figure 7 show examples of the topographic images and distribution of the neighbored peak pixels, indicating that most of the fibrous structures such as microfibrils were successfully labeled by neighbored peaks without being affected by the rough undulations of the surface of intact cell walls (Figs. 7a, c). In contrast, there were only a few labels on the relatively flat surface of the matrix components that embedded microfibrils in the inner surface (Fig. 7a) or on the granular matrix components that covered microfibrils in the outer surface (Fig. 7c) of the intact cell walls.

For the quantitative estimation of the effects of protease treatment on the exposure of the fibrous components of the cell wall surface, the ratios of the "neighbored peak points" of the intact and protease-treated cell wall surfaces were compared in the apical, intermediate, and cylindrical regions (Fig. 8). In all cases the ratio was significantly increased by the enzymatic treatment, indicating that the ratios could reflect the exposure of the microfibrils. Moreover, there were differences among the ratios depending on the cell wall region and these differences were consistent with the appearance of exposed microfibrils in the cell wall surface images. For example, the ratio from the inner surface of the intact cell wall was significantly higher in the cylindrical region than in other regions. This might be due to the presence of additional superficial microfibrils in the cylindrical region. In contrast, there were no significant differences among the regions in the inner surfaces of the protease-treated cell walls, probably

because the ridge extraction neglects the fine granular remnants of the matrix components (Fig. 7d). Although the matrix component coverage of the outer surfaces of intact cell walls was greater in the cylindrical region than in intermediate and apical regions, the differences were not reflected by the ratios (Fig. 8). This is apparently due to the fact that the ridge extraction, as shown in Fig. 7c, detected the neighbored peaks on the granular undulations, which were presumably the reflection of the fibrous structures such as microfibrils, as mentioned above.

Measurement of isolated microfibrils

Observations of negatively-stained, isolated cellulose microfibrils indicated that the microfibrils exhibited a ribbon-like configuration with fine longitudinal striations, along which the microfibrils were often separated into several subfibrils (Fig. 9a). The widths of the microfibrils were measured on fibrils that were not separated and the thicknesses were measured on points where the fibrils were twisted (*arrows* in Fig. 9a). As a result, the widths ranged from 7.9 nm to 48.8 nm, with an average of 26.8 nm (standard deviation, SD, 8.1 nm), and the thicknesses ranged from 1.9 nm to 7.2 nm with an average of 3.7 nm (SD 1.1 nm).

Topographic images of the isolated microfibrils were also obtained by atomic force microscopy (Fig. 9b). As diagrammed in Fig. 9c, the height and width of the microfibrils were measured from the profile along the 26 lines perpendicular to the longitudinal axes of the microfibrils, with the aid of the computer software. The measured heights averaged 7.3 nm (SD 4.7 nm) and ranged from 2.9 nm to 24.5 nm, whereas the widths averaged 28.7 nm (SD 7.7 nm) and ranged from 18.8 nm to 42.1 nm. Thus, the method for measurement the widths of the isolated microfibrils in topographic images

used in the present study provided similar results to those obtained from the direct observations of the negatively stained samples for transmission electron microscopy. However, the heights of microfibrils measured by atomic force microscopy varied considerably and were 2-fold greater than the thickness measured on the negatively-stained microfibrils by transmission electron microscopy.

Discussion

Structure of cell wall components

In the present study, cellulose microfibrils in both the inner and outer surfaces of the cell walls of *V. terrestris* were present in random directions with no recognizable regularity or specific pattern. Kataoka (1982), using a differential interference contrast microscope, reported the presence of longitudinal fibrous structures in the cylindrical region of cell walls isolated from *V. terrestris* cells. However, random microfibrils appeared in shadowed replicas of *V. sessilis* cell walls from which non-cellulosic components had been extracted chemically (Parker et al. 1963). Moreover, the present study indicates that microfibrils embedded deeply in matrix components are randomly arranged. Thus, the cell walls of *Vaucheria* spp. do not exhibit polylamellate structures in which microfibril orientations change regularly (Okuda et al. 1990; see Emons and Mulder 2000; Mulder and Emons 2001 for reviews). Since the cell expansion rates in meridional and radial directions in *V. terrestris* were not remarkably different in both living cells (Kataoka 1982) and isolated cell walls (Mine and Okuda 2003), the hypothesis that cell growth occurs perpendicular to the microfibril direction in

anisotropically growing cells of angiosperms (Shibaoka 1991) does not apply to *V. terrestris*. Therefore, the localized cell growth in the tip-growing *V. terrestris* must be controlled by cell wall factors other than mechanical anisotropy due to the microfibril orientation; for example, stress anisotropy in the domed growing tip reported in root hairs (Dumais et al. 2004).

In *V. terrestris*, the cell wall is much more extensible in the growing tip region than in the cylindrical, basal region and this extensibility is significantly dependent on environmental pH conditions (Mine and Okuda 2003). Treatment with protease weakens the cell walls in both the tip and cylindrical regions, since both the tensile stress required for cell wall extension and the amount of cell wall extension until rupture are concomitantly reduced (Mine and Okuda 2003). Since in this case the pH dependency of the cell wall extensibility remains even after protease treatment, it has been postulated that cell wall components act as two distinct factors, one involved in pH-dependent control of cell wall extensibility in the growing tip region of the cell and the other involved in the maintenance of cell wall strength in both the tip and cylindrical regions (Mine and Okuda 2003).

Both the transmission electron microscopy and atomic force microscopy images in the present study indicate the presence of amorphous or granular components embedding microfibrils in the inner surface and partially covering microfibrils in the outer surface of the cell wall. Ultrastructural studies of xyloglucans, a major matrix component in dicot plant cell walls, have been conducted using transmission electron microscopy of rapid-frozen, deep-etched replica specimens (McCann et al. 1990; 1991, Fujino et al. 2000). These studies have shown the thin, fibrous structures of xyloglucans that interconnect microfibrils. In the present study, no fibrous structures other than

microfibrils were observed.

However in *V. terrestris*, the observation that the matrix components are distributed throughout the cell and are removed by protease treatment strongly supports a significant role for these matrix components in the maintenance of cell wall strength. This is not in contradiction to the general belief that the mechanical properties of plant cell walls, such as extensibility and strength, largely depend on the nature of the matrix components and their interactions with the skeletal components (Fry 1986; Hayashi 1989, 1991; Cosgrove 1993, 1997).

We also have compared the configurations of cell wall components among apical (young, growing), intermediate, and cylindrical (old, mature) regions. The most noticeable difference observed in intact cell walls is that the coverage of the matrix components in the outer surface and the microfibrils in the inner surface both increase as the wall ages (compare the cylindrical, mature region in Fig. 3f with the apical and intermediate regions in Figs. 3d and e). This appears to explain the fact that the wall mechanical strength in the cylindrical region is greater than in the apical region (Mine and Okuda 2003). In the protease-treated cell walls, there were no significant differences in the configuration of the microfibrils among the cell wall regions; however atomic force microscopy images of inner surfaces of the apical cell walls showed remnants of the small granular components among the microfibrils. Since the pH dependency of the wall extensibility remained even in cell walls weakened by protease treatment (Mine and Okuda 2003), it might be possible that these protease-resistant components are involved in the pH-dependent control of cell wall extensibility in the apical, growing region.

Nature of the matrix components

The biochemical nature of the observed matrix components is unknown. The protease subtilisin *Carlsberg* (E.C.3.4.21.62) has been used to hydrolyze a variety of proteins but has not been reported to modify sugar chains. Therefore, it is probable that the enzyme removes the matrix components from the cell wall by hydrolyzing some structural protein(s). These structural protein(s) may be responsible for the regulation of the mechanical strength of the cell wall (Mine and Okuda 2003) and for the structural maintenance of the matrix components, as observed herein. Extensin is a major structural glycoprotein in angiosperms and is postulated to intensify the integrity of the cell wall by intermolecular cross-linking with itself or with other wall components (reviewed in Cassab 1998). It is possible that an extensin-like protein is present in *V. terrestris* cell walls and is involved in the integrity of the matrix components and the maintenance of cell wall strength.

In *V. terrestris*, since cellulose microfibrils are remarkably exposed after protease treatment of the cell wall, there exists a considerable volume of matrix components. This implies that the components are major cell wall constituents. It is generally known that plant cell walls have a certain amount of structural proteins, some of which interact with polysaccharide components (Carpita and Gibeaut 1993; Cassab 1998). If this is the case, the matrix components in the *V. terrestris* cell wall that are hydrolyzed by protease treatment are structural proteins and polysaccharides. According to an earlier monosaccharide analysis of differentially extracted polysaccharides from *V. sessilis* cell walls, the major constituents of polysaccharides extracted by hot water are glucose and some uronic acid(s). Subsequent alkaline extraction yielded no polysaccharides (Parker et al. 1963). Therefore, the matrix components in the present study may be composed of polysaccharides containing some glucans and/or uronans. Chi et al. (1999) reported the

localization of alginic acid, an acidic polysaccharide consisting of guluronic acid and mannuronic acid, in the outer layer of *V. germinata* cell walls by means of immunoelectron microscopy using an antibody specific for alginic acid. This indicates the possibility that the matrix components observed in the outer surface of the cell wall contain polysaccharides with an epitope similar to alginic acid.

Application of atomic force microscopy for observation of cell wall ultrastructure

Although a number of reports showing the arrangement of cellulose microfibrils in plant cell walls by atomic force microscopy have been published previously (e.g., Kirby et al. 1996; Round et al. 1996; Pesacreta et al. 1997; Thimm et al. 2000; Davies and Harris 2003), the present study is the first report of atomic force microscopy of algal cell walls. We have compared the appearance and structure of the inner and outer surfaces at sites that are distinct in age and growth activity, with and without protease that affects the mechanical properties of the cell wall. Moreover, we have used conventional specimen preparation techniques and transmission electron microscopy in order to examine the effectiveness of atomic force microscopy for ultrastructural studies of cell walls. Most of the morphological features of cell wall replicas observed with transmission electron microscopy were also observed in the topographic images obtained by atomic force microscopy. More detailed structures, such as the granular texture of matrix components, were detectable readily in atomic force microscopy images. Comparison of microfibril dimensions directly observed by transmission electron microscopy on negatively-stained specimens and those measured in topographic images indicate that the width of the ribbon-like microfibrils can be measured similarly with either technique. However the thickness as measured by atomic force microscopy is almost twice as large as that

measured in transmission electron microscopy specimens. At present, we have no clear explanation for these considerable differences in the measured thickness; however, they are most likely due to the difference in measurement technique, i.e., measurements on twisted points for transmission electron microscopy vs. line profiles for atomic force microscopy.

There are a number of additional advantages for atomic force microscopy of biological materials. For example, the costly apparatus and complicated procedures for shadowing and replica preparation are unnecessary for atomic force microscopy and the evaporation of bound water that can cause artificial deformations of fine structures is negligible under the atmospheric conditions used for atomic force microscopy. Thus, with atomic force microscopy we do not have to consider the possible morphological artifacts that are unavoidable with transmission electron microscopy in a high-vacuum environment with metal shadowing. This might be one reason why we can detect fine granular substructures of the matrix components by atomic force microscopy. Moreover, image contrast in transmission electron microscopy is dependent on the surface inclination of specimens in shadowed replicas, from which the specimen itself had been removed. In contrast, topographic images record the real height of the specimen surface in the presence of the specimen. This enables us to obtain, not only real topographic data that can be quantitatively evaluated, but also information about the physical and chemical characteristics of the specimen surfaces including antigenicity and viscoelastic features. Although there remain several disadvantages to atomic force microscopy, such as time-consuming observation and costly probes, atomic force microscopy has the potential to be one of the most effective tools for morphological studies of certain types of biological specimens. For example, the molecular structures of matrix polysaccharides

from plant cell walls have been observed by atomic force microscopy (Morris et al. 1997; Round et al. 2001). Combined with the data from our biochemical analysis, which is now in progress, it will be possible in the near future to visualize the interactions of the matrix and other cell-wall components from this alga and examine their significance in the mechanical properties of the cell walls.

Acknowledgements

We thank Dr. Hironao Kataoka, Tohoku University, for the gift of the algal strains and are grateful to Drs. Kazuhito Nishimura and Hideki Sasaoka, Industrial Technology Center of Kochi Prefecture, Japan, for generously providing the facilities for atomic force microscopy observations. We also thank Dr. Andy Round, University of Bristol, for critical reading of the manuscript.

References

Binnig G, Quate CF, Gerber C (1986) Atmic force microscope. Phys Rev Lett 56:930-933

Carpita NC, Gibeaut DM (1993) Structural models of primary cell walls in flowering plants: consistency of molecular structure with the physical properties of the walls during growth. Plant J 3:1-30

Cassab GI (1998) Plant cell wall proteins. Annu Rev Plant Physiol Plant Mol Biol 49:281-309

Chi E-S, Henry EC, Kawai H, Okuda K (1999) Immunogold-labeling analysis of alginate distributions in the cell walls of chromophyte algae. Phycol Res 47:53-60

Cosgrove DJ (1993) How do plant cell walls extend? Plant Physiol 102:1-6

Cosgrove DJ (1996) Plant cell enlargement and the action of expansins. BioEssays 18:533-540

Cosgrove DJ (1997) Relaxation in a high-stress environment: the molecular bases of extensible cell walls and cell enlargement. Plant Cell 9:1031-1041

Cosgrove DJ (1999) Enzymes and other agents that enhance cell wall extensibility. Annu Rev Plant Physiol Plant Mol Biol 50:3971-3417

Davies LM, Harris PJ (2003) Atomic force microscopy of microfibrils in primary cell walls. Planta 217: 283–289

Dumais J, Long SR, Shaw SL (2004) The mechanics of surface expansion anisotropy in Medicago truncatula root hairs. Plant Physiol. 136: 3266-3275.

Emons AM, Mulder BM (2000) How the deposition of cellulose microfibrils builds cell wall architecture. Trends Plant Sci 5:35-40

Fry SC (1986) Cross-linking of matrix polymers in the growing cell walls of angiosperms. Annu Rev Plant Physiol 37:165-186

Fujino T, Sone Y, Mitsuishi Y, Itoh T (2000) Characterization of cross-links between cellulose microfibrils, and their occurrence during elongation growth in pea epicotyl. Plant Cell Physiol 41:486-494

Hayashi T (1989) Xyloglucans in the primary cell wall. Annu Rev Plant Physiol Plant Mol Biol 40:139-168

Hayashi T (1991) Biochemistry of xyloglucans in regulating cell elongation and expansion. In: Lloyd CW (ed) The cytoskeletal basis of plant growth and form. Academic Press, London, pp 131-144

Hörber JKH, Miles MJ (2003) Scanning probe evolution in biology. Science

302:1002-1005

Kataoka H (1982) Colchicine-induced expansion of *Vaucheria* cell apex. Alternation from isotropic to transversally anisotropic growth. Bot Mag Tokyo 95:317-330

Kataoka H (1987) The light-growth response of *Vaucheria*. A conditio sine qua non of the phototropic response? Plant Cell Physiol 28:61-71

Kirby AR, Gunning AP, Waldron KW, Morris VJ, Ng A (1996) Visualization of plant cell walls by atomic force microscopy. Biophys J 70:1138-1143

Kutschera U (1991) Regulation of cell expansion. In: Lloyd CW (ed) The cytoskeletal basis of plant growth and form. Academic Press, London, pp 149-158

Masuda Y (1990) Auxin-induced cell wall loosening. Bot Mag Tokyo 103:345-370

McCann MC, Wells B, Roberts K (1990) Direct visualization of cross-links in the primary plant cell walls. J Cell Sci 96:323-334

McCann MC, Wells B, Roberts K (1991) Complexity in the spatial localizeion and length distribution of plant cell-wall matrix polysaccharides. J Microscopy 166:123-136

Mine I, Okuda K (2003) Extensibility of isolated cell walls in the giant tip-growing cells of the xanthophycean alga *Vaucheria terrestris*. Planta 217:425-435

Morris VJ, Gunning AP, Kirby AR, Round A, Waldron K, Ng A (1997) Atomic force microscopy of plant cell walls, plant cell wall polysaccharides and gels. Int J Biol Macromolecules 21: 61-66

Morris VJ, Gunning AP, Kirby AR (2005) Atomic force microscopy for biologists. Imperial College Press, London

Mulder BM, Emons AM (2001) A dynamical model for plant cell wall architecture formation. J Math Biol 42:261-289

Nishitani K (1997) The role of endoxyloglucan transferase in the organization of plant

cell walls. Int Rev Cytol 173:157-206

Okuda K, Matsuo K, Mizuta S (1990) Characteristics of the deposition of microfibrils during formation of the polylamellate walls in the coenocytic green alga *Chamaedoris orientalis*. Plant Cell Physiol 31:357-365

Park YW, Tominaga R, Sugiyama J, Furuta Y, Tanimoto E, Samejima M, Sakai F, Hayashi T. (2003) Enhancement of growthby expressin of poplar cellulase in *Arabidopsis thaliana*. Plant J 33:1099-1106

Parker BC, Preston RD, Fogg GE (1963) Studies of the structure and chemical composition of the cell walls of Vaucheriaceae and Saprolegniaceae. Proc Roy Soc B 158: 435-444

Pesacreta TC, Carlson LC, Triplett BA (1997) Atomic force microscopy of cotton fiber cell wall surfaces in air and water: quantitative and qualitative aspects. Planta 202: 435-442

Rose JKC, Braam J, Fry SC, Nishitani K (2002) The XTH family of enzymes involved in xyloglucan endotransglucosylation and endohydorolysis: Current perspectives and a new unifying nomenclature. Plant Cell Physiol 43:1421-1435

Round AN, Kirby AR, Morris VJ (1996) Collection and processing of AFM images of plant cell walls. Microscopy and Analysis 55:33-35

Round AN, Rigby NM, MacDougall AJ, Ring SG, Morris VJ (2001) Investigating the nature of branching in pectin by atomic force microscopy and carbohydrate analysis. Carbohydr Res 331:337-342

Shibaoka H (1991) Microtubules and the regulation of cell morphogenesis by plant hormones. In: Lloyd CW (ed) The cytoskeletal basis of plant growth and form. Academic Press. London, pp 159 - 168

Thimm JC, Burritt DJ, Ducker WA, Melton LD (2000) Celery (*Apium graveolens* L.) parenchyma cell walls examined by atomic force microscopy: effect of dehydration on cellulose microfibrils. Planta 212: 25-32

Updegraff DM (1969) Semimicro determination of cellulose in biological materials. Anal Biochem 32:420-424.

Figure legends

Fig 1. Cell wall specimen of *Vaucheria terrestirs* and the regions observed. **a-c** Light micrographs showing how the apical portions of cell wall fragments were turned inside-out. A glass needle (NL) with a tip diameter of about 40 μm was inserted into the apical portion of the cell wall fragment (CW) through an opening (OP) made with a razor 0.2-0.4 mm behind the apex. Shaded area represents inner surface of cell wall. The apical portion of the cell wall fragment was tucked up, using a pig hair from a paint brush, until the needle tip reached the furthest tip of the cell wall. A second glass needle with a thinner tip (about 10 μm in diameter; NS) was placed on a micromanipulator in the opposite direction (**a**). The thinner needle was moved to the thicker needle until the tip came in contact with the apical cell wall on the thicker needle tip (**b**). The apical portion of the cell wall was inverted over the thinner needle by tucking up to the opposite side while the furthest tip of the cell wall was immobilized between the tips of the two needles. This resulted in the apical portion of the cell wall being turned completely inside-out, allowing direct access to the inner surface of the cell wall (**c**). The *arrow* in (**b**) indicates the direction in which the apical portion of the cell wall was tucked up. **d** A light micrograph of a cell wall fragment mounted on a cover slip and a probe with a cantilever seen as a

dark tapered object, taken with the built-in CCD camera of the scanning probe microscope. The *arrow* indicates the apex of the cell wall fragment. Note that the inside-out apical cell wall fragment is situated distal to the cut end (*arrowhead*). **e** Diagrammatic representation of the three regions of an apical cell wall fragment. A, B, and C are the apical, intermediate, and cylindrical regions, respectively

Fig. 2. Inner surface of cell wall fragments without protease treatment. *Arrow* cell wall matrix components with fine granular appearance embedding cellulose microfibrils in deeper layer . **a-c** Topographic images obtained by atomic force microscopic at apical (**a**), intermediate (**b**), and cylindrical (**c**) regions. Scale bar (200 nm) in **a** also applies for **b** and **c**. Image heights were 76, 104, and 78 nm, respectively. **d-f** Transmission electron micrographs of shadowed replicas at apical (**d**), intermediate (**e**), and cylindrical (**f**) regions. Scale bar (200 nm) in **d** also applies for **e** and **f**

Fig. 3. Outer surfaces of cell wall fragments without protease treatment. **a-c** Topographic images at apical (**a**), intermediate (**b**), and cylindrical (**c**) regions. Scale bar (200 nm) in **a** also applies for **b** and **c**. Image heights were 88, 93, and 89 nm, respectively. **d-f** Shadowed replicas at apical (**d**), intermediate (**e**), and cylindrical (**f**) regions. Scale bar (200 nm) in **d** also applies for **e** and **f**

Fig. 4. Inner surfaces of cell wall fragments treated with protease. **a-c** Topographic

images at apical (**a**), intermediate (**b**), and cylindrical (**c**) regions. Scale bar (200 nm) in **a** also applies for **b** and **c**. Image heights were 50, 56, and 68 nm, respectively. **d-f.** Shadowed replicas at apical (**d**), intermediate (**e**), and cylindrical (**f**) regions. *Arrow* a dark hole or cleft where metal had not been evaporated during shadowing. Scale bar (200 nm) in **d** also applies for **e** and **f**

Fig. 5. a-c Topographic images of outer surfaces of cell wall fragments treated with protease at apical (**a**), intermediate (**b**), and cylindrical (**c**) regions. Scale bar (200 nm) in **a** also applies for **b** and **c**. Image heights were 60, 52, and 65 nm, respectively

Fig. 6. Three-dimensional renderings of 250 x 250-nm portion of the topographic images. **a-h** Transformed from trimmed images of Figs. 2a, 2c, 3a, 3c, 4a, 4c, 5a, and 5c, respectively. **a-d** Intact cell walls: inner surfaces at apical (**a**) and cylindrical (**b**) regions; outer surfaces at apical (**c**) and cylindrical (**d**) regions. **e-h** Protease-treated cell walls: inner surfaces at apical (**e**) and cylindrical (**f**) regions; outer surfaces at apical (**g**) and cylindrical (**h**) regions

Fig. 7. Examples of image pairs obtained from ridge detection of topographic images. Left: Images after a 4-fold reduction of resolution. Right: Black and white images in which positions of “neighbored peaks” are shown as black pixels. **a** Inner surface of the apical region of an intact cell wall fragment. Note that neighbored peaks were detected

along the superficial cellulose microfibrils, but not on the granular components that embed deeper microfibrils. **b** Inner surface of the cylindrical region of a protease-treated cell wall. **c** Outer surface of the cylindrical region of an intact cell wall. Note that neighbored peaks were not detected on the irregular granular structures that cover microfibrils. **d** Outer surface of the apical region of a protease-treated cell wall. Image heights were 233, 58, 93, and 63 nm, respectively. Neighbored peak ratios were 20.3%, 39.6%, 21.9%, and 34.8%, respectively. Scale bar (200 nm) in **a** also applies for **b** and **c**

Fig. 8. Neighbored ridge ratios of topographic images. The averages of the ratios of the inner and outer surfaces of the cell-wall fragments of the apical, intermediate, and cylindrical regions are represented by thick vertical bars. White and black bars are the ratios from intact and protease-treated cell walls, respectively. Vertical lines represent the standard deviations. Three to 11 images were analyzed for each, with an average of 6.5 images analyzed

Figs. 9. Images of isolated cellulose microfibrils. **a** Transmission electron micrograph of negatively-stained microfibrils. *Arrow* the twisted portions of microfibrils where the thicknesses were measured. **b** Topographic image obtained by atomic force microscopy. Image height was 61 nm. Scale bars are 200 nm. **c** A line profile for the measurement of microfibril dimensions. Actual width of the image was 85.9 nm and the height was 11.0 nm. A: Outline of a cross-section of a microfibril. B: Baseline of the microfibril drawn manually. C: The perpendicular line from the point farthest from the baseline to the

baseline. The distance between the point and the foot of the perpendicular line was used as the microfibril height. D: The halfway line between the point and the bottom line. The distance between the intersections of this line and the microfibril outline was the microfibril width

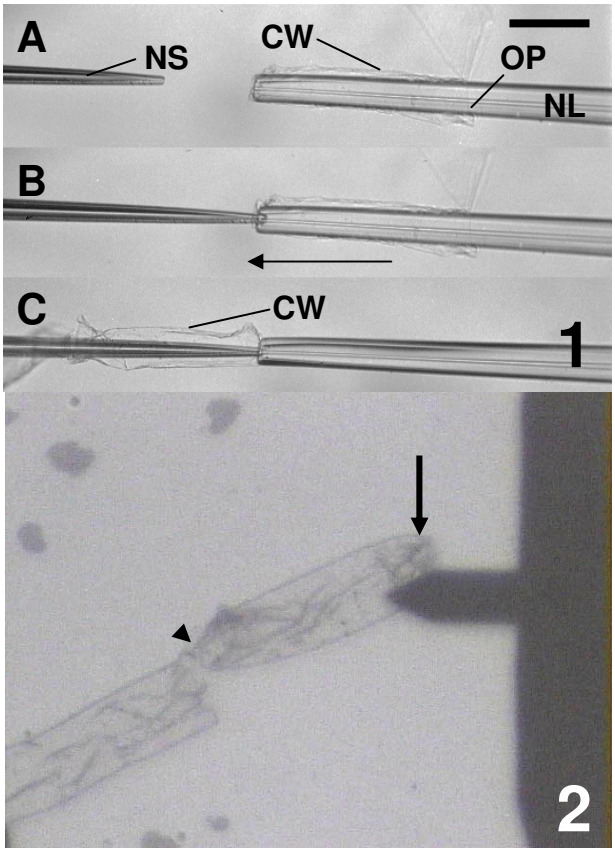
A
NS
CW
OP
NL
B
C
CW
1
2

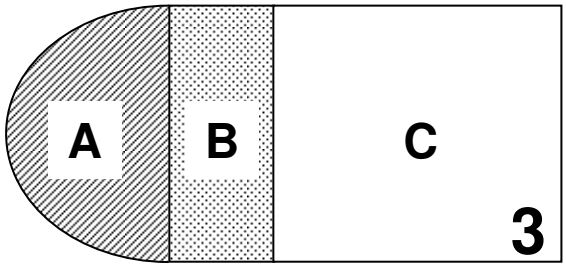
A
B
C
3

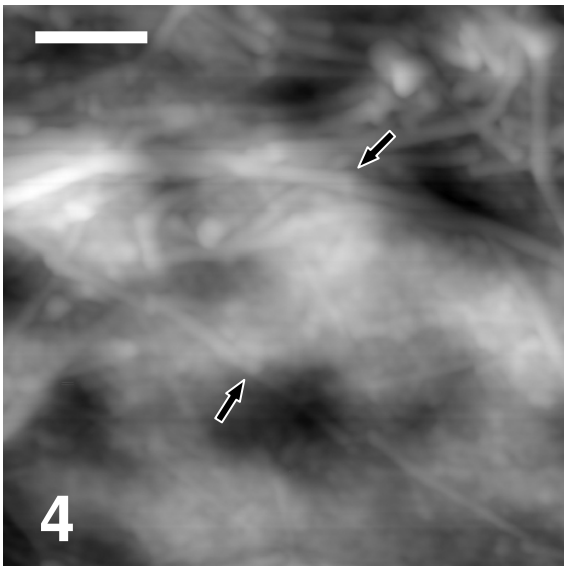
4

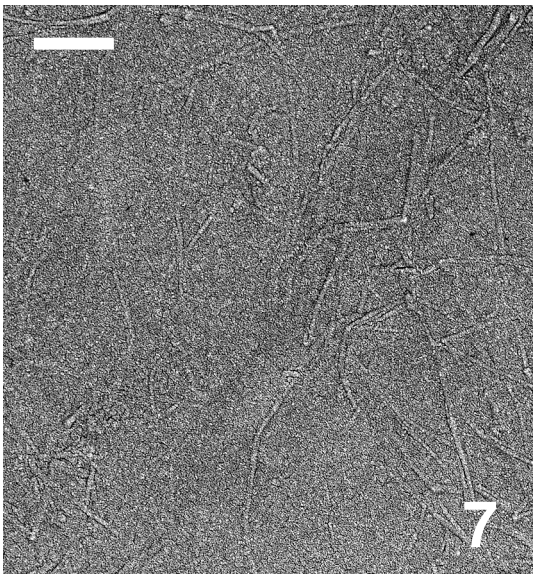
7

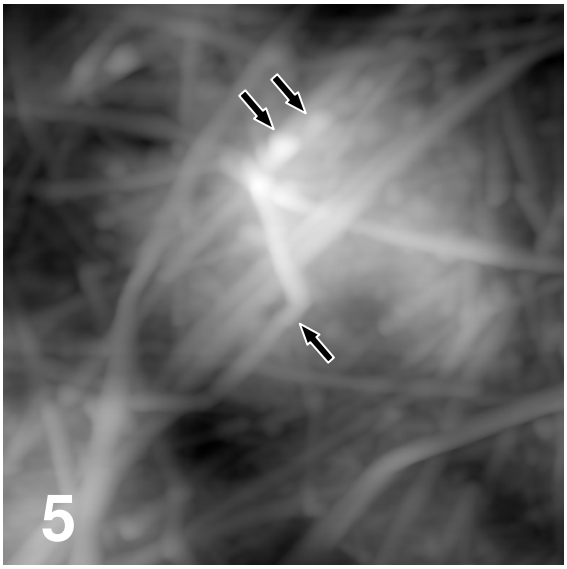
5

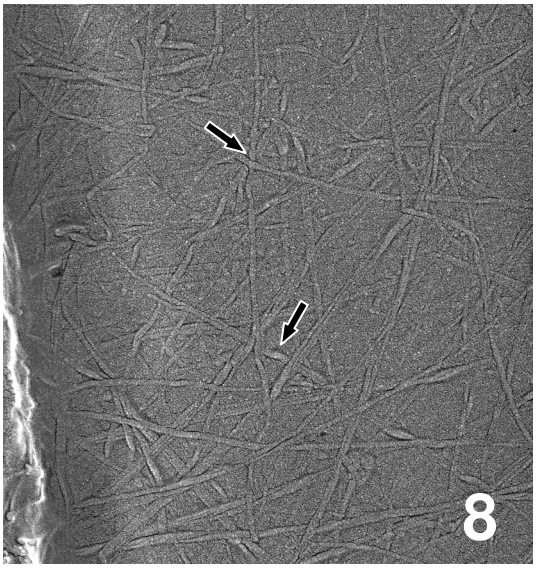
8

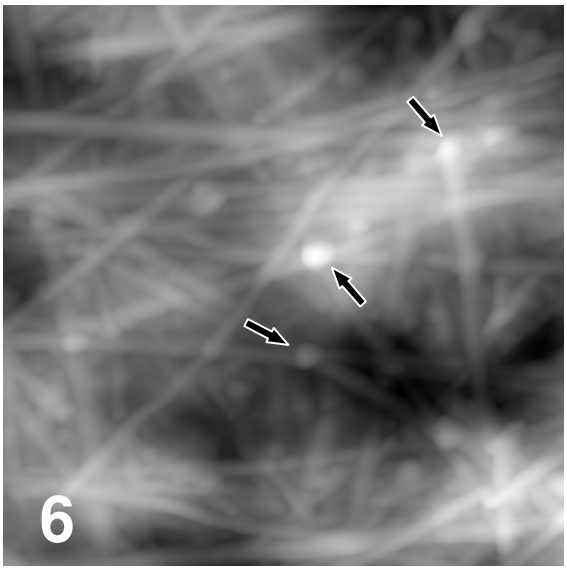
6

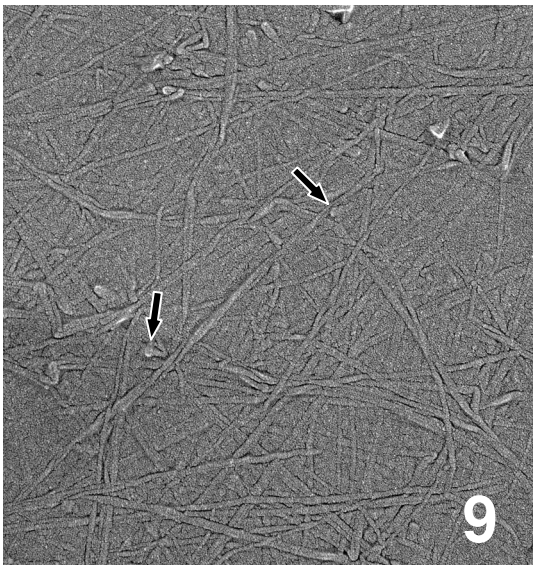
9

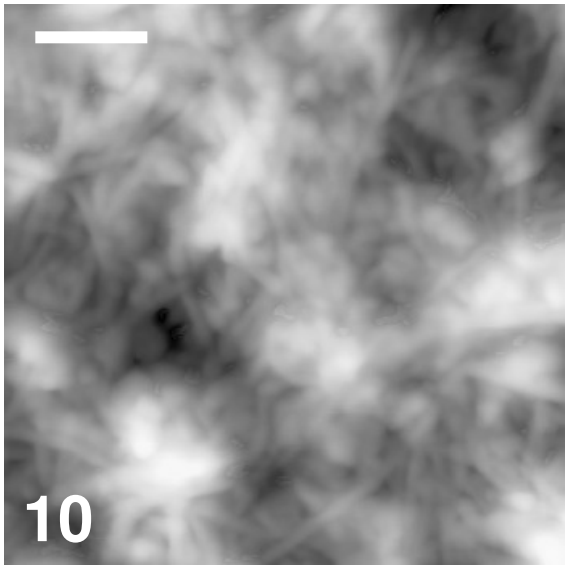
10

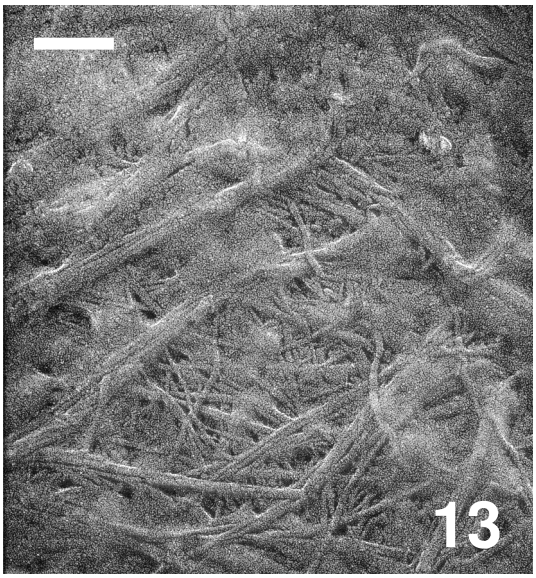
13

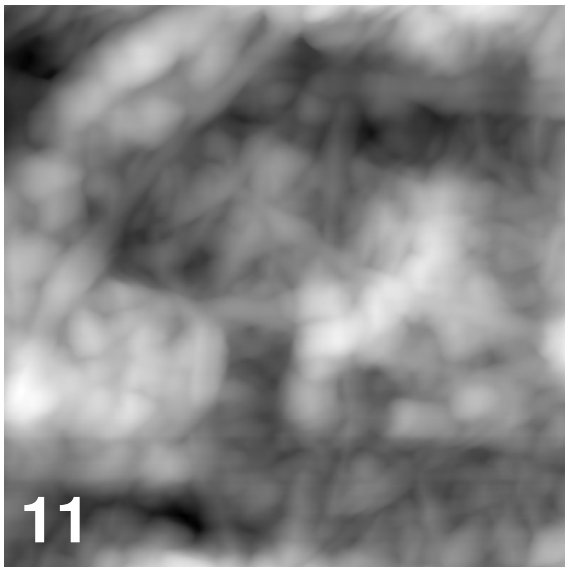
11

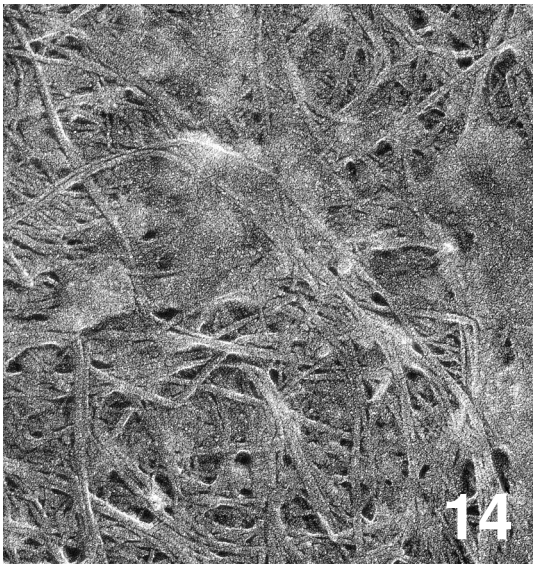
14

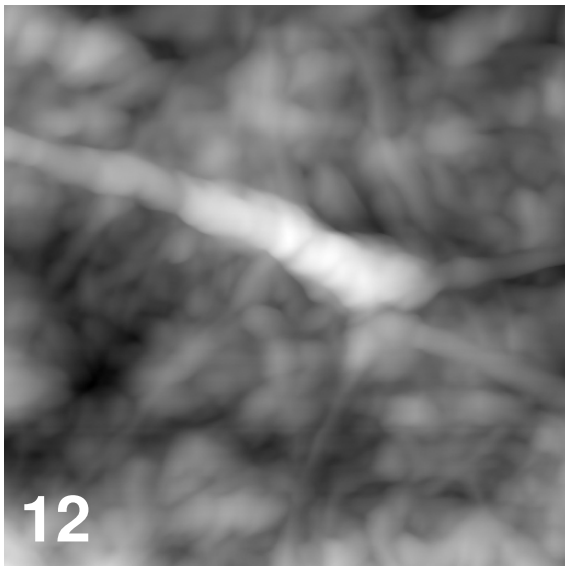
12

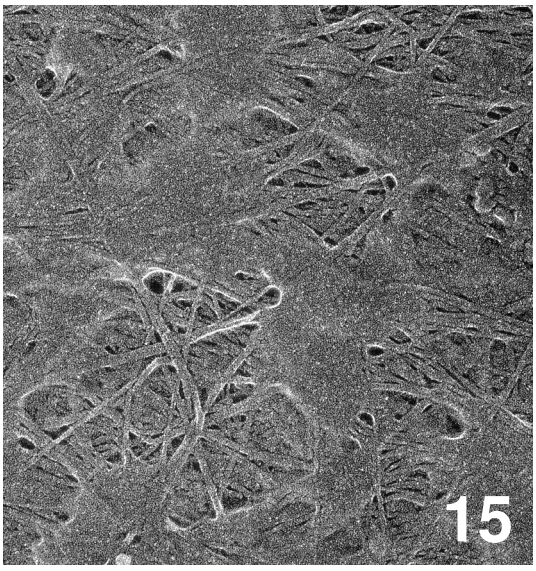
15

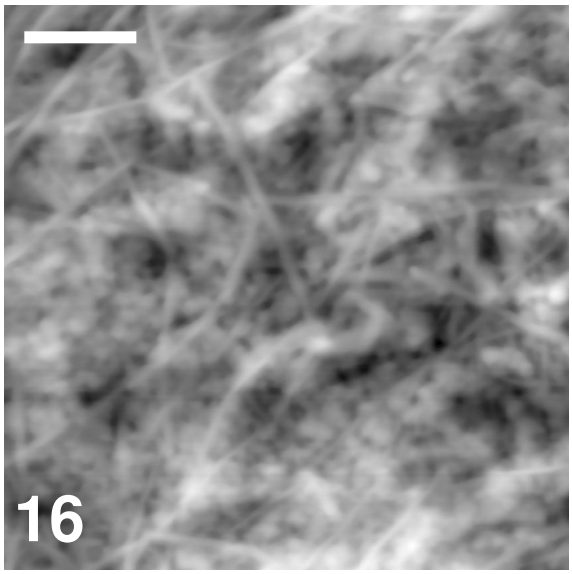
16

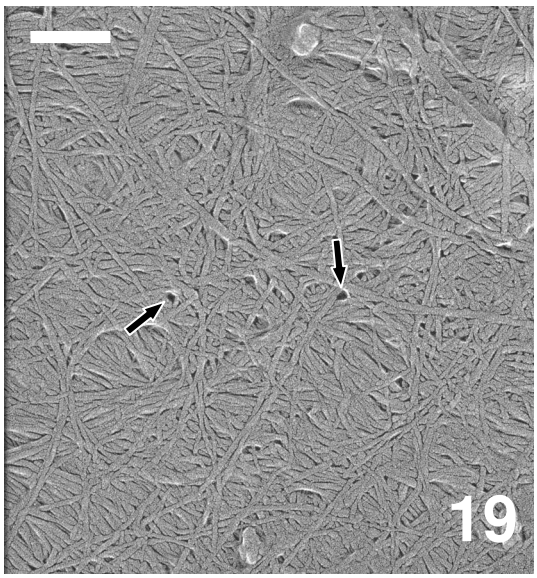
19

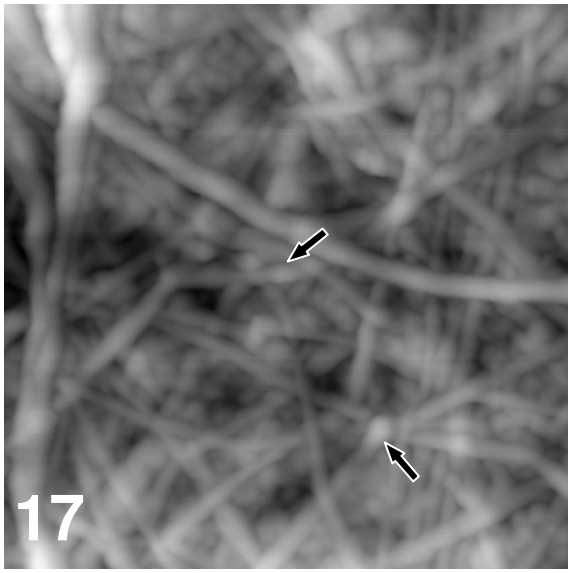
17

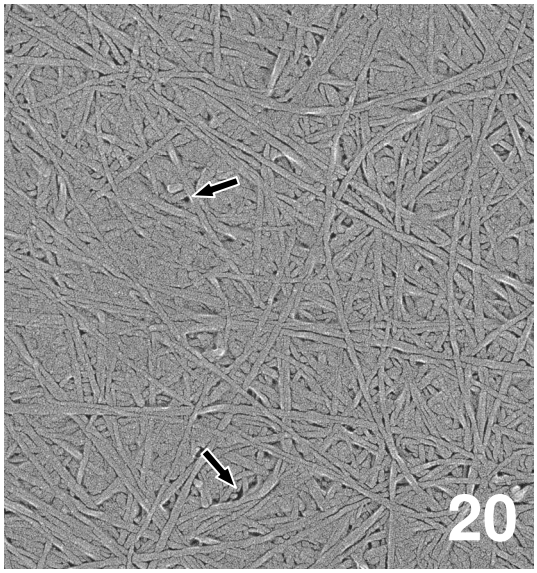
20

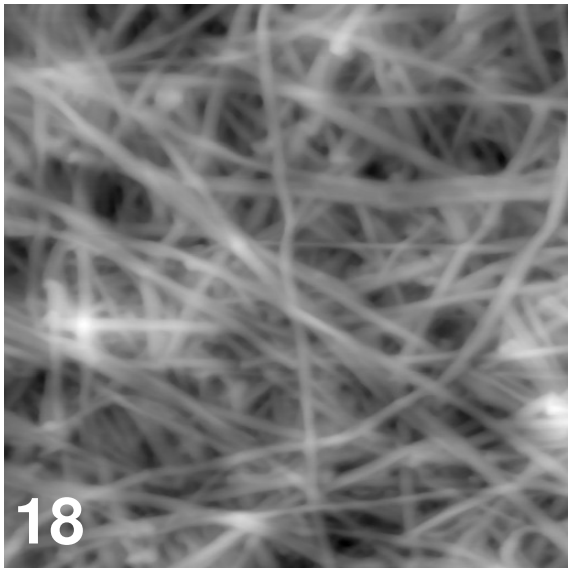
18

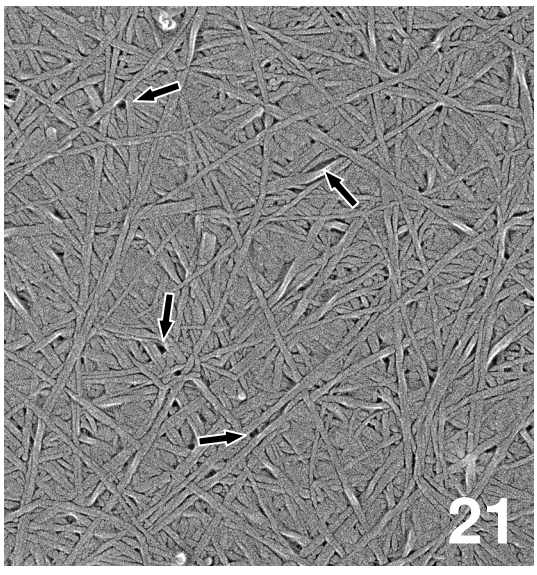
21

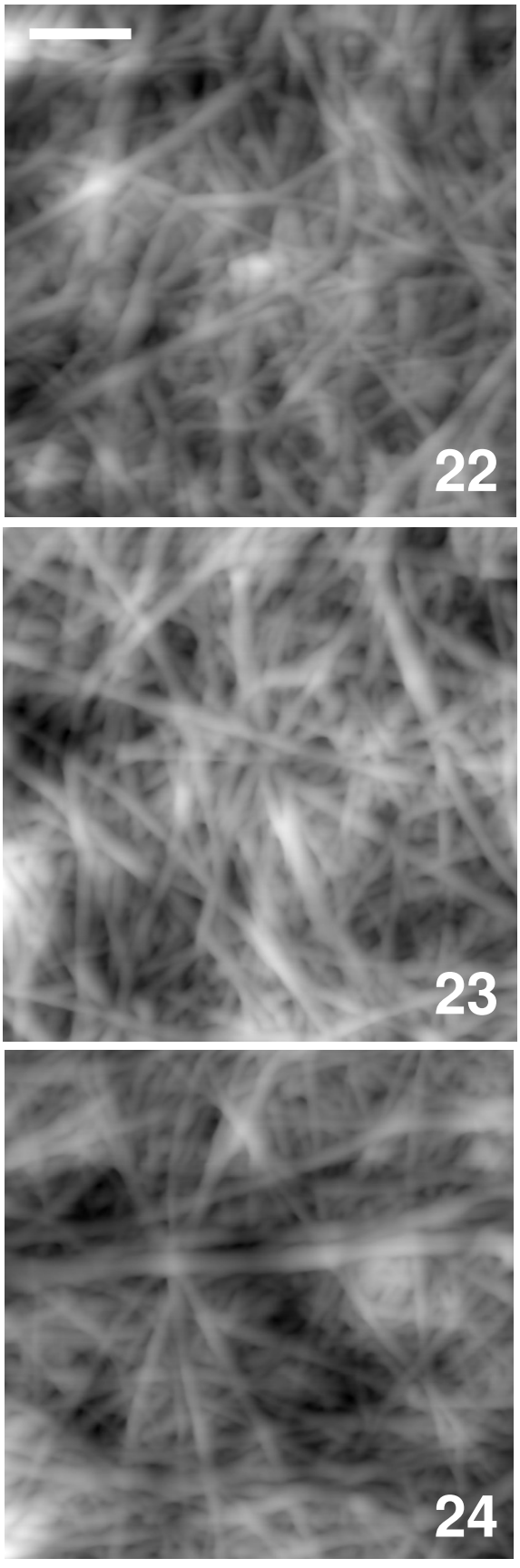
22
23
24

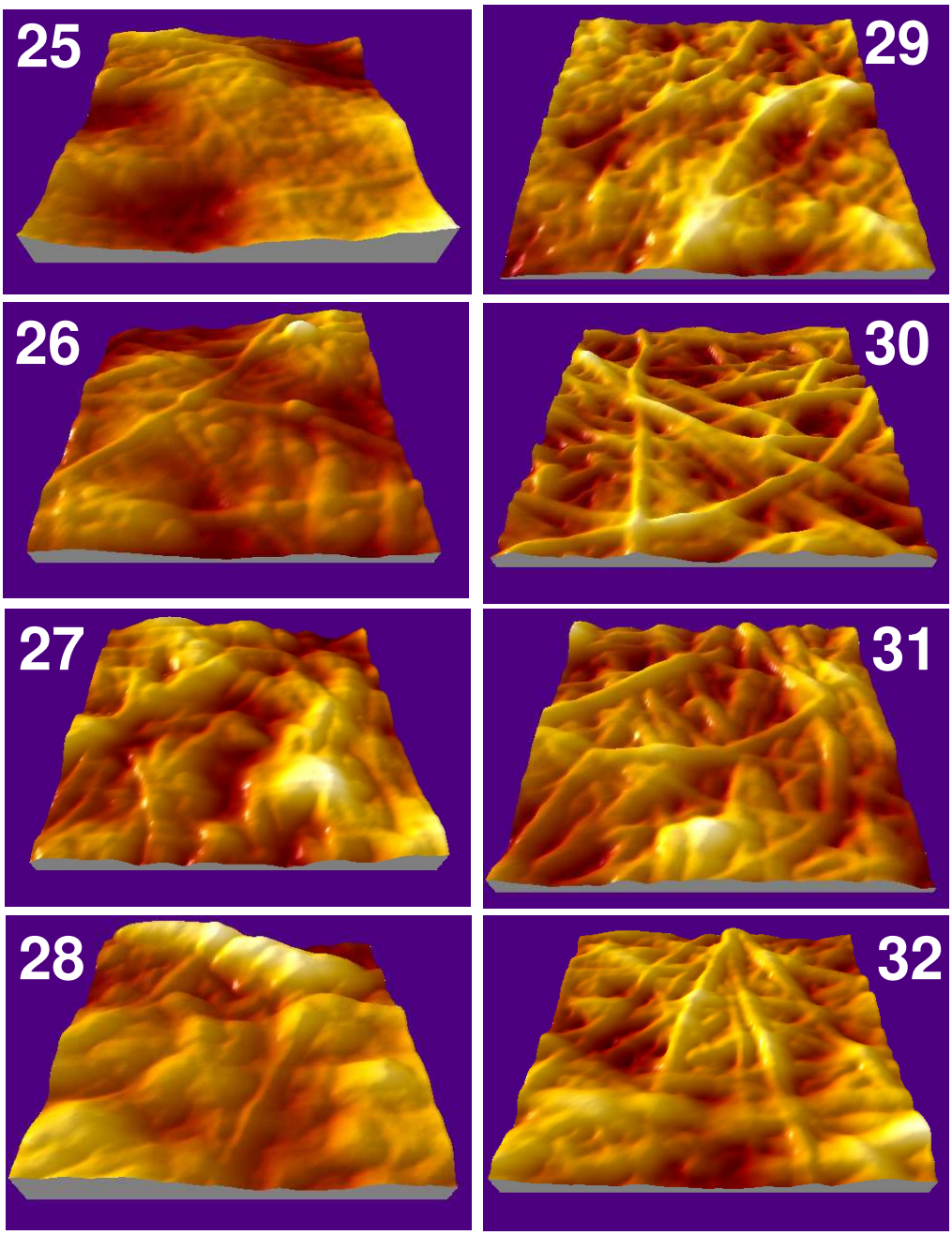
25
29
26
30
27
31
28
32

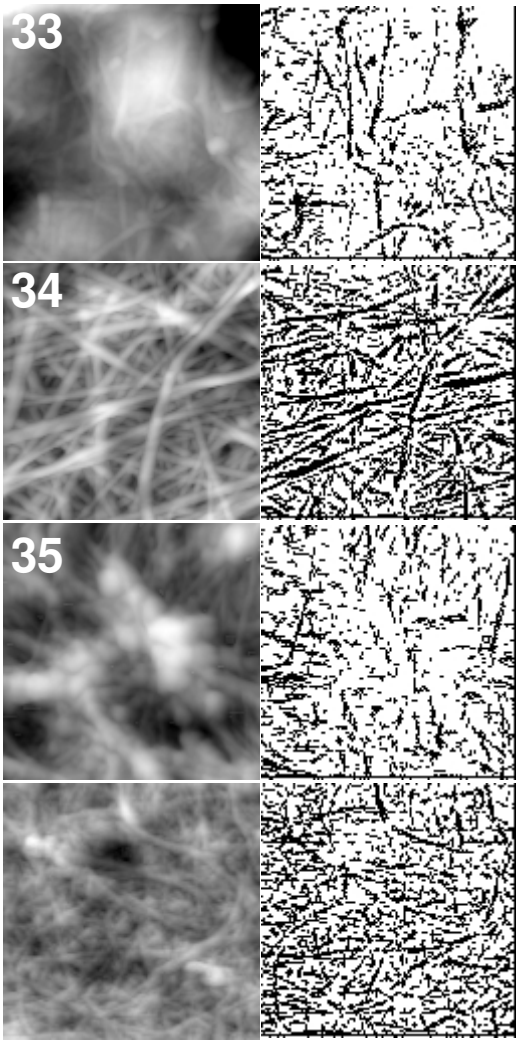
33
34
35

```
ERROR: stackunderflow
OFFENDING COMMAND: ~

STACK:
```